OmniInput: An Evaluation Framework for Deep Learning Models on Internet-Scale Data

Anonymous authors
Paper under double-blind review

Abstract

Evaluating machine learning models is important yet challenging in many real-world scenarios. Traditional analysis is dataset-driven, that is, models are evaluated on predefined benchmark datasets. However, these datasets can only cover a limited scope, leaving *unanticipated* inputs untested and weaknesses of the model unrevealed. To overcome this problem, we propose OmniInput, a novel approach to evaluate models comprehensively using an input space (i.e. internet-scale data). Our method entails efficient sampling of the inputs from the model and estimation of its corresponding output distribution, and an innovative way to calculate the model's precision and recall curve from the output distribution with only modest human annotation effort. In our experiments, we first validate the correctness of OmniInput within a small input space where brute-force enumeration is still possible. We then show that OmniInput can quantitatively evaluate more complex models such as language models (various versions of GPT2, OLMo, and DistilBERT) and computer vision models, and analyze interesting patterns in an input space.

1 Introduction

Traditional ways of evaluating machine learning (ML) models mostly rely on the use of a pre-defined dataset (Dosovitskiy et al., 2021; Tolstikhin et al., 2021; Steiner et al., 2021; Chen et al., 2021; Zhuang et al., 2022; He et al., 2015; Simonyan & Zisserman, 2014; Szegedy et al., 2015; Huang et al., 2017; Zagoruyko & Komodakis, 2016; Liu et al., 2020; Hendrycks & Gimpel, 2016; Hendrycks et al., 2019; Hsu et al., 2020; Lee et al., 2017; 2018; Liang et al., 2018; Mohseni et al., 2020; Ren et al., 2019; Cao et al., 2022; Sun & Li, 2022; Szegedy et al., 2013; Rozsa et al., 2016; Miyato et al., 2018; Kurakin et al., 2016; Xie et al., 2019; Madry et al., 2017). Depending on how these datasets are constructed, many of them can only cover a limited scope among all possible inputs. Models tested against pre-defined datasets might generalize poorly to unseen inputs in a real-world scenario; hence the weaknesses of the model remain unnoticed. For example, data collected in a lab environment cannot certify the performance of real-world environment which tends to have more out-of-distribution data. This problem becomes more severe as large language models (LLMs) have become widely accessible to the public, allowing users to input virtually any type of prompt, potentially causing the models to behave unpredictably.

To overcome this issue, we propose to evaluate models comprehensively using Internet-scale data from the models' own input spaces with equal importance. Without loss of generality, we consider models with a discrete and finite *input space* in this work. For example, the input space of a large language model can be all token sequences with low perplexity (i.e. human-understandable sequences).

Note that brute-force enumeration in such input spaces is typically computationally impossible. An alternative approach is to uniformly sample data from the internet and evaluate the model's predictions on these inputs. However, this uniform sampling strategy is also impractical for a large number of potential inputs because models typically do not predict with high confidence on most of these inputs. They would assign high confidence to the inputs that they believe are familiar with, such as those from their training distribution.

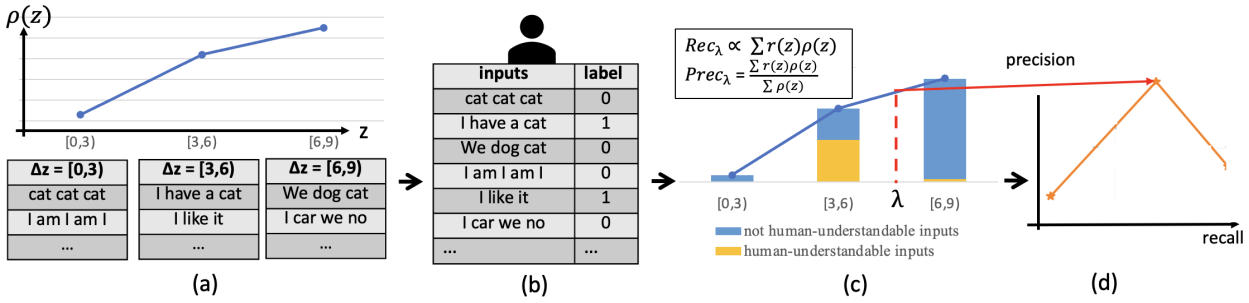

Figure 1: An overview of our novel OmniInput framework for language models as an example. (a) Use an efficient sampler to obtain the output distribution $\rho(z)$ and the sampled inputs for each bin Δz; (b) Annotate the sampled inputs; (c) Calculate the precision and recall at different thresholds λ that distinguish different classes. $r(z)$ denotes the precision of the model within the bin of output value z; (d) Construct a precision-recall curve.

To tackle this challenge of comprehensive model evaluation without a dataset, we propose OmniInput, a novel approach to calculate the precision and recall curve of a model over an input space with reasonable human annotation effort. The key to estimating the precision and recall where enumeration of the input space is impossible lies in the *output distribution* of the model (Liu et al., 2023). The output distribution is the proportion of inputs that corresponds to each output value [1], showing the (relative) difference in the number of inputs for different outputs (e.g., 10% of inputs have output equal to 1, 25% of inputs have output equal to 2, etc.). Specifically, we first sample the inputs and estimate the output distribution of the model under evaluation. We then calculate the model's precision and recall at different output values using the output distribution and selective annotations, putting together a precision-recall curve over the input space. As shown in Fig. 1, it consists of four steps:

(a) We employ a well-established sampling and histogram reweighting algorithm (Hukushima & Nemoto, 1996; Swendsen & Wang, 1986) to obtain the output distribution $\rho(z)$ of a trained model (where z denotes the output value of the model), and efficiently sample the inputs from different output value bins (e.g., negative-log-likelihood or NLL for language models). In an open-world setting without any prior knowledge of the samples, all possible inputs in the input space should be evaluated with equal importance.

(b) We annotate the sampled inputs. Using language models as an example, we rate how likely the inputs are understandable sentences using a score from 0 to 1 for language models. This is in contrast to the traditional dataset-driven evaluation setting where the entire testing dataset is annotated beforehand. Annotations in our scheme take place *after* the output distribution is sampled. Because the sampling algorithm reliably selects representatives from all possible inputs given an output value, our annotations can be done on a *limited, incomplete* input space, while offering insights more meaningful and relevant to the model itself.

(c) We compute the precision for each bin as $r(z)$, then estimate the precision and recall at different threshold values λ. When aggregating the precision across different bins, a weighted average of $r(z)$ by the output distribution $\rho(z)$ is required. See Sec. 2.2 for details.

(d) We finally put together the precision-recall curve for a comprehensive evaluation of the model performance.

OmniInput makes it possible to compare different models beyond pre-defined datasets selected from a limited input space. The resulting precision-recall curve can help decide the limit of the model in real-world deployment. A model with a high Area Under the Precision-Recall (AUPR) curve in OmniInput is expected to agree closely with human expectations. As OmniInput evaluates the model by having the test

[1] For language models, we use the log-perplexity (or negative-log-likelihood) as the output. We do not treat them as language generators but as language modelers, where a good language model should assign higher scores (low perplexity) to inputs that humans see as reasonable and fluent, and low scores (high perplexity) to inputs that are nonsensical or unreasonable. For computer vision models in MNIST, logit can be used as the output value to be sampled from.

data sampled uniformly from the input space, it eliminates possible human biases introduced by the test data collection process (Luo et al., 2023; Prabhu et al., 2023; Shu et al., 2020; Leclerc et al., 2022).

We first validate the correctness of OmniInput on a model with a small input space where brute-force enumeration is still possible. We then conduct extensive experiments using OmniInput to evaluate different models with a large input space where brute-force enumeration becomes impossible. Specifically, we show that OmniInput applies to (large) language models, such as GPT2 (Radford et al., 2019), OLMo (Groeneveld et al., 2024), and DistilBERT (Sanh, 2019) for text sentiment classification. We also provide an in-depth analysis of computer vision models on the MNIST dataset. All these experiments lead to interesting and sometimes surprising observations. For example, a generative model with a ResNet architecture correctly learns the patterns of the digit "1." However, its recall is significantly lower than that of a simpler multi-layer perceptron classifier, which instead learns "1" by merely inverting the foreground and background of the digit "0." This means the metrics defined in this work (precision and recall) are not indicative of which training method or model architecture is better, Instead, they prioritize other aspects (e.g. reasoning ability, alignment with human intuition, safety, etc) when comparing models. Hence OmniInput, as a proof of concept, paves the way for future research that seeks to better evaluate models by incorporating aspects other than just accuracy.

Our new contributions are:

- We propose a novel dataset-free framework, OmniInput, to evaluate machine learning models by estimating the precision-recall curve of the model.
- Our novel evaluation paradigm samples the test data from the model's input space, which goes beyond the use of pre-defined datasets. It includes all possible evaluation perspectives and eliminates possible human biases introduced by the test data collection process.
- OmniInput leverages the output distribution of a model to carefully select a reasonable number of representative samples for humans to annotate. This can reduce human effort in the annotation process, while covering a larger and unbiased input space.
- We empirically validate the correctness of OmniInput and show that it can evaluate various popular (large) language models and computer vision models, and provide detailed analysis.

2 The OmniInput Framework

We now present the details about sampling the output distribution across the input space, and introduce the OmniInput framework to evaluate model performance by calculating precision and recall in its input space.

2.1 Output Distribution and Sampler

Output Distribution. We denote a trained neural network as $f : \mathbf{x} \to z$ where $\mathbf{x} \in \Omega_T$ is the training set, $\Omega_T \subseteq \{0, ..., N\}^D$, and $z \in \mathbb{R}$ is the output value that the model assigns to an input. In the example of Natural Language Processing (NLP), z is the NLL which is the log of perplexity. Depending on the task, other outputs could be used. Each of the D tokens takes one of the $N+1$ values. The **output distribution** represents the frequency count of each output z given the (entire) input space $\Omega = \{0, ..., N\}^D$ or some other space Ω_M specified by a model M. The output distribution represents the occurrence for each output value z. Following the principle of equal *a priori* probabilities in statistics, we assume that each input within Ω occurs equally likely. Therefore, in our framework, each input is equally important for analysis and evaluation. In practice, the statistics of sampling is saved with a histogram $H(z)$, which stores the occurrence of each output value z:

$$H(z) = \sum_{\mathbf{x} \in \Omega} \delta(z - f(\mathbf{x})),$$

where $\delta(\cdot)$ is 1 if $z - f(\mathbf{x})$ is 0, or $\delta(\cdot)$ is 0 otherwise.

The sampled inputs (also called **representative inputs**) predicted with similar output values near z in a small range $[z - \Delta z, z + \Delta z)$ are mapped to the same z bin. Δz is a small positive constant chosen empirically.

The output distribution $\rho(z)$ is then obtained by normalizing the histogram, that is,

$$\rho(z) = \frac{H(z)}{\sum_z H(z)}. \tag{1}$$

Discrete Input Sampling and Text Generation. Markov Chain Monte-Carlo (MCMC) for sampling discrete inputs from ML models are recently proposed (Grathwohl et al., 2021; Zhang et al., 2022). These samplers sample from an ML model to yield a target distribution

$$p_T(\mathbf{x}) \propto \exp(g(\mathbf{x})/T), \tag{2}$$

where $g(\cdot)$ is the negative "energy" and T is a temperature. The sampler initializes a sequence $\mathbf{x}$ of random tokens (or pixels for image inputs). The sampling proceeds by switching some tokens (or pixels) of the sequence to "denoise", and the goal is to acquire the distribution preferred by large $g(\mathbf{x})$. $p_T(\mathbf{x})$ is a quantity dependent on temperature T. When T is 1, $g(\cdot)$ becomes the log-probability, a common quantity to be modeled in machine learning (LeCun et al., 2006). $p_T(\mathbf{x})$ in Equ. 2 is also a widely used target distribution in computer vision (Goshvadi et al., 2024) for image generation and natural language processing for text generation (Kumar et al., 2022; Qin et al., 2022).

Samplers. Parallel Tempering (PT) (Hukushima & Nemoto, 1996; Swendsen & Wang, 1986) and Histogram Reweighting (HR) (Ferrenberg & Swendsen, 1989) is an efficient approach to obtain output distribution. They are compatible and can take advantage of the development of MCMC samplers that sample from ML models. PT begins with running multiple Metropolis samplers (Metropolis et al., 1953) at different temperatures T simultaneously. The samplers exchange configurations at intervals to accelerate mixing and the thermalization/denoising procedure. Samples are collected by the samplers individually to yield their corresponding target distributions $p_T(\mathbf{x})$. HR then reweighs the sampled distributions and combines them to yield the model's output distribution, which is independent of T and only dependent on the definition of the model itself.

2.2 Calculation of Precision-Recall

OmniInput revolves around the *output distribution* $\rho(z)$ to formulate the *estimation* of the precision-recall, when combined with additional information from annotated sampled inputs. The samplers described in the previous step provide us with the output distribution, as well as the sampled inputs. For a language model, these sampled inputs are text sequences with N tokens each. We can then proceed to the annotation of these inputs, and use them to calculate the precision and recall.

Annotation of Inputs. Our motivation is to quantify how much a model's prediction agrees or deviates from humans' perception, hence humans serve as a gold standard for comparison. For each "bin" of the output distribution (recall that each "bin" collects the inputs with a small range of output values $[z - \Delta z, z + \Delta z)$, a subset of the sampled inputs is selected for annotation and scored by a human. This score ranges from 0 when the sample completely deviates from the annotator's judgment for the target class, to 1 when the prediction from the model perfectly agrees with the annotator's judgment (input with "**good**" prediction). Following the evaluation, the average score for each bin, termed "precision per bin", $r(z)$, is calculated. It is the proportion of the total evaluation score on the inputs (analogous to true positives) relative to the total number of inputs (analogous to true and false positives) within that bin. The number of bins ranges from 150 to 600, depending on the specific experiments in our study.

Precision and Recall (PR)[2]. For our experiments on language models, we use the NLL as the output z for sampling, because it is the loss of the next-token prediction. A low NLL corresponds to a human-understandable sentence. We define a varying threshold of model confidence λ such that the inputs predicted with $z \leq \lambda$ by the model are similar to their training data, i.e., they are regarding by the model as human-understandable sentences. Thus, the precision given λ is defined as

$$\text{precision}_\lambda = \frac{\sum_{z \leq \lambda} r(z)\rho(z)}{\sum_{z \leq \lambda} \rho(z)}. \tag{3}$$

[2]Another commonly used metric, the Receiver-Operating Characteristic (ROC) curve, is closely connected to PR (see Appendix A).

The numerator is the *true positives* which estimates the number of "good" predictions and the denominator is the total number of inputs predicted as positives – the sum of true positives and false positives. This denominator can be interpreted as the *area under curve* (AUC) of the output distribution from the $-\infty$ to threshold λ. A higher precision indicates a higher proportion of the inputs agreeing with annotators' judgments for the given output values.

To compute the recall, we need the total number of ground truth inputs that are positives over the entire input space Ω. This number is a constant, albeit unknown. Hence the recall is proportional to $\sum_{z\leq\lambda} r(z)\rho(z)$:

$$\text{recall}_\lambda = \frac{\sum_{z\leq\lambda} r(z)\rho(z)}{\text{number of positive inputs}} \propto \sum_{z\leq\lambda} r(z)\rho(z). \tag{4}$$

A higher recall indicates that the model makes more predictions that agree with the annotators' judgments. As demonstrated above, the output distribution is a valuable quantity for deriving both precision and unnormalized recall. These metrics can be used to understand the model's mapping by varying the threshold λ. To simplify the calculation, when $\rho(z)$ differs significantly for different z, precision_λ is approximated as $r(z^*)$ where $z^* = \arg\max_{z\geq\lambda} \rho(z)$ and recall_λ is approximately proportional to $\max_{z\geq\lambda} r(z)\rho(z)$.

For the binary classifiers, both (very) negative and (very) positive logit values correspond to the (high) confidence predictions for different classes, separated by the logit=0 which corresponds to probability 0.5 when Sigmoid activation is used. In this case, we need to designate one class, and the lower and upper limits of the summation in Equ. 3 and Equ. 4 should be set accordingly.

2.3 Application: Model Comparison

One application of OmniInput is to compare models by PR calculated based on each model's own sampled inputs, that reflect the distribution and composition of representative inputs over different output values. The two models M_1 and M_2 can be compared based on their respectively sampled inputs and *normalized* output distributions.

Both of the following normalization techniques can be used. *Entire output distribution normalization* needs to sample the output distribution of all the output values. *Cross-models normalization* is fast but it needs to post-process the output distributions of two models and it can only compare two models.

Entire output distribution Normalization. To facilitate a meaningful comparison of different models based on their output distribution, we can use Equ. 1 to acquire the output distribution. This normalization samples the output distribution of (all) possible output values to ensure the *normalization* can be calculated as accurately as possible. We leverage the fact that the entire input space contains an identical count of $(N+1)^D$ samples for all models under comparison Landau et al. (2004). where $\hat{\rho}(z)$ denotes the unnormalized output distribution.

Cross-models normalization. To achieve the comparison, we first designate an input subspace from the original input space, such as the subspace whose inputs have their corresponding outputs predicted by both models within a certain range of $\mathbb{Z} = [z_-, z_+]$: $\mathbb{X} = \{\mathbf{x} | M_1(\mathbf{x}) \in \mathbb{Z} \text{ and } M_2(\mathbf{x}) \in \mathbb{Z}\}$. During sampling for M_1, we acquire a sampled unnormalized output distribution $\rho_{M_1}(z)$ and the sampled inputs for each z. Feeding the sampled inputs from M_1 to both models, we find a subset of inputs $\mathbb{X}_{M_1}$ that are from $\mathbb{X}$, meaning that the predicted outputs $z_1, z_2 \in \mathbb{Z}$ for both model when $z_1 = M_1(\mathbf{x})$ and $z_2 = M_2(\mathbf{x})$. We repeat this process for M_2 and acquire $|\mathbb{X}_{M_2}|$ as the number of sampled inputs from M_2 but these inputs are predicted by both models in $\mathbb{Z}$. We can therefore get the normalized output distributions as

$$\hat{\rho}_{M_1}(z) = \frac{H_{M_1}(z)}{|\mathbb{X}_{M_1}|} \ , \tag{5}$$

$$\hat{\rho}_{M_2}(z) = \frac{H_{M_2}(z)}{|\mathbb{X}_{M_2}|} \ . \tag{6}$$

Both $\hat{\rho}_{M_1}$ and $\hat{\rho}_{M_2}$ are directly comparable, because $\mathbb{X}$ is shared by both of the models. In practice, having $\mathbb{Z}$ is also preferable because not all output values are interesting to consider. For example, a large NLL mostly corresponds to noisy inputs and they generally have very small precision.

As an intuitive example of validation of normalization, suppose it is enumerable to have ground truth count in a large input space where model M_1 maps 500 inputs to outputs within $\mathbb{Z}$ and Model M_2 maps 200 inputs within $\mathbb{Z}$. $\mathbb{X}$ is the set of inputs that are predicted by both models within $\mathbb{Z}$. $\mathbb{X}$ has 100 inputs.

We sample 50 inputs with outputs within $\mathbb{Z}$ by M_1, and it is expected to have around 10 of them from $\mathbb{X}$, because the sampled proportion $\frac{50}{10}$, should be close to the ground truth proportion $\frac{500}{100}$. Therefore, Equ. 5 is $\frac{50}{10} = 5$. We then sample 50 inputs whose outputs are within $\mathbb{Z}$ by M_2, and we should have around 25 of them from $\mathbb{X}$. The sampled proportion Equ. 6 is $\frac{50}{25} = 2$, close to the ground truth proportion $\frac{200}{100} = 2$. Therefore, comparing the sampled proportions 5 versus 2 computed from Equ. 5 and Equ. 6 of is as if we were comparing the ground truth count of 500 versus 200.

3 OmniInput Experiments on Natural Language Processing

3.1 Experimental settings

We first apply OmniInput to a **Toy** example where enumeration of all inputs is affordable to confirm OmniInput's correctness (Sec. 3.2). In Sec. 3.3, OmniInput is used in two pre-trained GPT2 models (Radford et al., 2019) and OLMo models (Groeneveld et al., 2024) with sequence length 25. We also apply OmniInput to longer sequences of length 100 in GPT-2 models. The sampling target is the training loss, the negative-log-likelihood (NLL), used for next-token predictions. Finally, we also apply OmniInput to a sentiment classifier.

3.2 Toy example validates accuracy of sampling results

Toy is a simple GPT2 model with 4 attention heads and 6 layers. We train it to generate a sequence of 8 tokens, each token is an integer between 0 to 9. That is, $\mathbf{x} = \{x_1, x_2, ..., x_8\}$, where $x_i \in \{0, 1, ..., 9\}$. We put a constraint to require the sum of the 8 tokens to be divisible by 30: $(\sum_{i=1}^{8} x_i)$ mod 30 $= 0$. Therefore, the input space has 10^8 inputs, which is enumerable. Our trained model can generate all sequences that satisfy the division-by-30 constraint. Fig 2 shows the resulting $r(z)$ and $\rho(z)$ compared to the ground-truth enumeration, which confirms that they are very close to each other. This provides confidence in extending the approach to more complex applications.

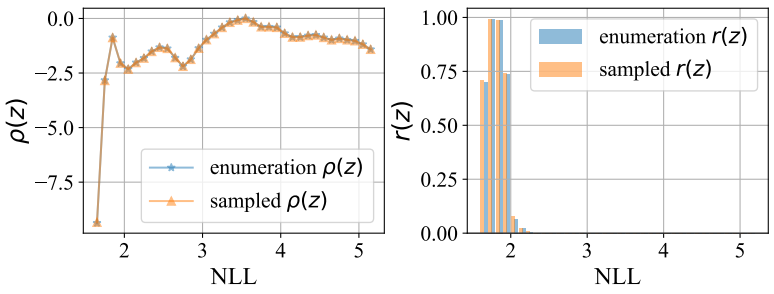

Figure 2: Toy example where enumeration is affordable. The line plot (left) and the bar plot (right) show that our sampling results match the ground truth for both output distribution $\rho(z)$ and precision per bin $r(z)$, respectively.

3.3 OmniInput evaluation on real-world (large) language models

We apply OmniInput to pretrained GPT-2 and OLMo models to evaluate their performance. Specifically, we test two versions of GPT-2: GPT-2 medium with 25 tokens, referred to as GPT2-medium-25, and GPT-2 small with 25 tokens, referred to as GPT2-small-25. To examine these models' performance on longer sequences, we also test them on 100 tokens, denoted as GPT2-medium-100 and GPT2-small-100, respectively. For larger models, we apply OmniInput to four pretrained OLMo models with 25 tokens, OLMo-7B, OLMo-1B, OLMo-7B-SFT, and OLMo-7B-Instruct. We use the default vocabulary sizes of 50,304 for OLMo models and 50,257 for GPT-2 models. We emphasize that a test set is not required, as OmniInput does not rely on a predefined dataset for evaluation. Unlike the controlled toy experiments, enumeration is neither assumed nor feasible in real-world applications.

We sample the inputs for different NLL values. A low NLL indicates that the model strongly believes that the sequence is similar to the training distribution (e.g. human-understandable sentences). However, it was

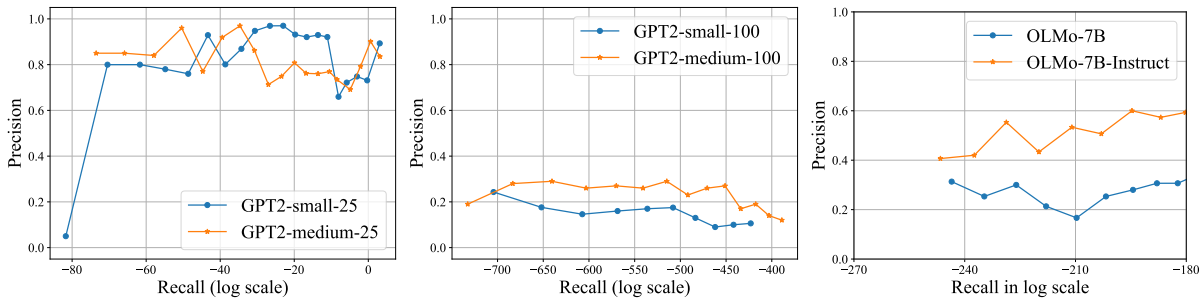

(a) GPT2 with seqlen 25. (b) GPT2 with seqlen 100. (c) OLMo 7B(-Instruct) with seq len 25.

Figure 3: Precision-Recall (PR) Curves for Different Language Models.

found that sequences with NLL below a certain threshold start to contain repeating words and are difficult to be understood by humans (Holtzman et al., 2019). Therefore, we empirically choose an NLL output range and only consider their corresponding inputs when calculating precision and recall (PR). We select the lower bound of the NLL value when it is associated with at least 30 non-duplicate input sequences; the upper bound is constrained by our available human annotation resources. The valid NLL range varies for different models, so we label the inputs with different NLL ranges in different settings. In the GPT2-small-25 and GPT2-medium-25 experiments, we label the inputs with NLL ranging from 2.0 to 4.0. For GPT2-small-100 and GPT2-medium-100, we annotate the outputs with NLL ranging from 4.0 to 5.0. For OLMo models, the NLL range for OLMo-1B is 3.2 to 4.1; 3.4 to 4.3 for OLMo-7B, 3.7 to 4.6 for OLMo-7B-Instruct, and 3.5 to 4.4 for OLMo-7B-SFT. Each bin captures $\Delta\text{NLL} = 0.1$.

Precision-Recall (PR) Curves and Model Performance. Fig. 3 shows that OmniInput can be applied to produce PR curves for different models and sequence lengths. The PR curves for the two GPT2 models with sequence length 25 demonstrate that these settings generally lead to highly understandable sequences, as indicated by the high precision (see Fig. 3(a)). The results suggest that the two models achieve comparable precision and recall for a sequence length of 25.

We also quantitatively compare the area under the PR curve (AUPR) with respect to the (log-scale) recall (x-axis). A larger AUPR means that the model's predictions agree better with human perspective. First we find the common minimum and maximum recall of the two PR curves for GPT2-small-25 and GPT2-medium-25 respectively, and compute the (linear) interpolation of the precision (y-axis) at each recall. We then accumulate the area starting from the common minimum recall and compare the proportion of the AUPRs for the two PR curves. The AUPR of GPT2-medium-25 is then divided by the AUPR of GPT2-small-25. As an example, the proportion of the cumulative AUPR ending at log-recall around 2 (largest recall) is 1.015, indicating the predictions of GPT2-medium-25 agree slightly better with human annotations.

For sequence lengths of 100, OmniInput indicates that GPT2-medium-100 outperforms GPT2-small-100 within the selected output range Z for the language modeling task. The PR curves of both GPT2 models for sequence length 100 shows that both models generate sequences that are difficult to understand, because of the low precision (see Fig. 3(b)). The PR curve for GPT2-medium-100 is almost always above the PR curve for GPT2-small-100. GPT2-medium has a larger AUPR and thus performs better than GPT2-small for sequence length 100, though both of them have low precision in general.

For OLMo models, OmniInput indicates that OLMo-7B-Instruct outperforms OLMo-7B for sequence lengths of 25 for language modeling task. OLMo-7B-Instruct has a higher precision than OLMo-7B's in a similar recall range, so integrating the PR curve of OLMo-7B-Instruct results in a higher AUPR compared to that of OLMo-7B (see Fig. 3(c)). Therefore, the sequences from OLMo-7B-Instruct are easier to understand. Because the tokenizers are different, we cannot compare across different models.

Insights from Representative Inputs. An in-depth analysis by scrutinizing the inputs raises some concerns about privacy leaking and hallucination. For example, an input we encountered contains some company names with their addresses. An internet search on these names or addresses seems to not match, suggesting a potential privacy leak. Another example is a sequence of magic keywords "Good morning dear

friend, I, and Greetings, ladies and gentlemen". GPT2-small-25 keeps generating email addresses before this sequence. This raises a concern of privacy leaking of the models.

For GPT2-small-100, we can sample NLL down to around 2.7 where we find repeating words similar to sentences with NLL smaller than 2 in GPT2-small-25. When NLL gets higher, the repeating phrases are generally more meaningful, such as "pickup truck pickup 4 trailer trailer" or "put clean clothes put things wash clothes." Overall, sentences with 100 tokens in the selected NLL range have repeated words and are generally not fluent. More experimental details are in Appendix H. Based on our observations, we speculate that the next-token generation ability of these models, driven by a sophisticated next-token generation function, may not fully align with the NLL for an entire sentence.

3.4 Language classifier

We fine-tune a DistilBERT (Sanh et al., 2019) model using the SST2 dataset (Socher et al., 2013) and achieve 91% accuracy. We choose the logits as our sampling target, and evaluate this model using OmniInput. Since the maximum length of SST2 is 66 tokens, one can define the input space for DistilBERT to be sentences with exactly 66 tokens. For shorter sentences, the last few tokens are padded with padding tokens. Because a typical sentence in SST2 contains 10 tokens, we therefore evaluate sentences of 66 tokens in length and 10 tokens in length, respectively.

OmniInput finds that the language classifier performs poorly, as the precision is 0 for all the recall values. Analysis on the sampled inputs for each positive logit bin reveals that the model tends to classify primarily based on specific keywords, rather than understanding the grammar and structure of the sentences. Appendix C contains more sampled inputs for different sentence lengths.

Because OmniInput focuses on using PR as the performance metric, it is therefore able to discover the weakness of the model, i.e., disagreement with human's understanding of a meaningful sentence. When the input space contains out-of-distribution (OOD) inputs, it is understandable that the language classifier performs poorly because it is trained to predict the conditional probability $p(class|\mathbf{x})$ given $\mathbf{x}$ are from the training distribution. To handle an open-world setting where OOD's are ubiquitous, the models must also learn to distinguish whether the inputs are from the training distribution.

In summary, our method offers a comprehensive approach to performance assessment. OmniInput is able to capture how well the model's predictions align with human perspective for two reasons: (i) the human annotation process in OmniInput takes place *after* the sampled inputs are determined. The sampled inputs are dissimilar from the training data and have a better chance to reveal "corner cases" or OOD's. (ii) OmniInput evaluates both the precision and recall of the model, which are not used in the loss function during the training procedure. They therefore provide a completely different perspective from the training loss as performance metrics.

4 OmniInput Experiments on Computer Vision

We also apply OmniInput to computer vision tasks, demonstrating its versatility across different modalities. In all computer vision experiments, we focus on binary classifiers and energy-based generative models, both of which produce scalar outputs. For classifiers, we consider positive output values (positive logits) $\log p(y = 1|\mathbf{x})$, and for energy-based generative models, we consider log-likelihoods (larger output values).

4.1 Experimental settings

We evaluate several backbone models for computer vision: convolution neural network (**CNN**), multi-layer perceptron network (**MLP**), and **ResNet** (He et al., 2015). The details of the model architectures are provided in Appendix D. We extract only the inputs with labels $\{0, 1\}$ from the MNIST training set to build the classifiers and refer to this reduced training set as **MNIST-0/1**. We also evaluate generative models for ResNet and MLP. To train these generative models, we select only the inputs with **label=1** as **MNIST-1**; inputs with labels other than **label=1** are considered **OOD** inputs. We train these models using different training methods: (1) Using the vanilla binary cross-entropy loss, we train classifiers **CNN-MNIST-0/1**

and **MLP-MNIST-0/1**[3] which achieve test accuracy of 97.87% and 99.95%, respectively. (2) Using the binary cross-entropy loss and data augmentation by adding uniform noise with varying levels of severity to the input images, we train **RES-AUG-MNIST-0/1**, **MLP-AUG-MNIST-0/1**, and **CNN-AUG-MNIST-0/1** which achieve test accuracy of 99.95%, 99.91%, and 99.33%, respectively. (3) Using energy-based models that learn by generating inputs, we train **RES-GEN-MNIST-1** and **MLP-GEN-MNIST-1**[4].

4.2 Traditional evaluation is not comprehensive

Traditional dataset evaluation depends on the datasets we choose, so it is inherently not comprehensive. Specifically, we use five different test sets for MNIST binary classifiers by fixing the *positive test samples* as the samples in the MNIST test set with label=1, and varying the *negative test samples* in five different ways: (1) the inputs in the MNIST test set with **label=0** (**in-dist**), and **OOD** inputs from other datasets: (2) **Fashion MNIST** (Xiao et al., 2017), (3) **Kuzushiji MNIST** (Clanuwat et al., 2018), (4) **EMNIST** (Cohen et al., 2017) with the "byclass" split, and (5) **Q-MNIST** (Yadav & Bottou, 2019).

Table 1: Traditional evaluations: AUPR scores on pre-defined test sets with five different types of negative samples (see for details), leading to inconsistent evaluation results for model ranking.

	in-dist	out-of-distribution (OOD)			
Model	MNIST label=0	Fashion MNIST	Kuzushiji MNIST	EMNIST	QMNIST
CNN-MNIST-0/1	99.81	98.87	93.93	79.42	13.84
RES-GEN-MNIST-1	99.99	**100.00**	**99.99**	**99.87**	**16.49**
RES-AUG-MNIST-0/1	**100.00**	99.11	93.93	95.10	15.69
MLP-MNIST-0/1	**100.00**	99.42	92.03	90.68	15.81

Precision-Recall Curves over the Entire Input Space. As indicated by the AUPR scores in Table 1, predefined test sets like those mentioned above rarely yield consistent model rankings during evaluation. For example, RES-GEN-MNIST-1 performs the best on all the test sets with OOD inputs while only ranked 3 out of 4 on the in-distribution test set. CNN-MNIST-0/1 outperforms MLP-MNIST-0/1 on Kuzushiji MNIST, but it typically performs the worst on other test sets. Additional inconsistent results using other evaluation metrics can be found in Appendix E.

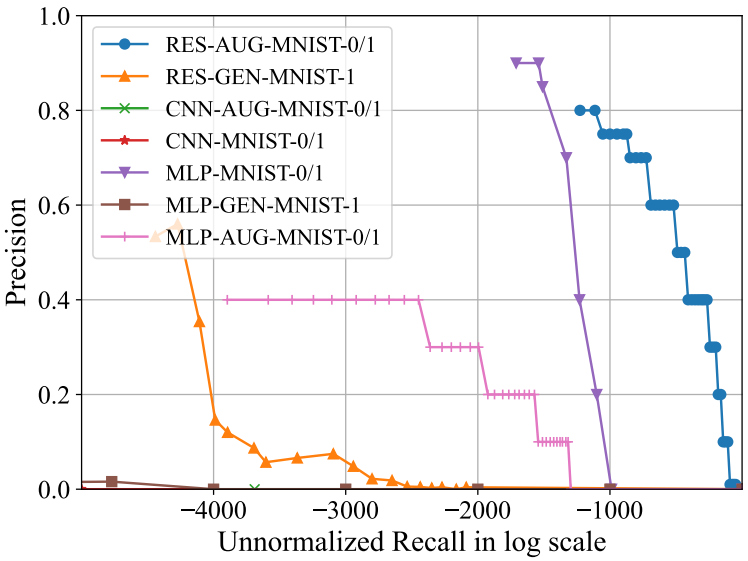

Figure 4: OmniInput evaluation: Precision-Recall curves obtained by OmniInput for various computer vision models in this study. See main text for the model details. Some models (CNN-AUG-MNIST-0/1, CNN-MNIST-0/1, MLP-MNIST-0/1) have 0 precision.

4.3 OmniInput evaluation

Fig. 4 presents a comprehensive precision-recall curve analysis using OmniInput. The results of OmniInput suggest that RES-AUG-MNIST-0/1 is the best model and MLP-MNIST-0/1 is the second best, both having relatively high recall and precision scores. RES-GEN-MNIST-1, as a generative model, displays a low recall but relatively good precision. Notably, CNN-MNIST-0/1 and CNN-AUG-MNIST-0/1 exhibit almost no precision greater than 0, indicating that "hand-written" digits are rare in the representative inputs even when the logit value is large (see Appendix G). This suggests that these two models are seriously subjected to an overconfident pre-

[3]RES-MNIST-0/1 is omitted due to reported sampling issues in ResNet (Liu et al., 2023).
[4]CNN-GEN-MNIST-1 cannot learn to generate reasonable images because the model complexity is low.

diction problem where the models map the obviously wrong inputs (e.g. noisy inputs) over-confidently as "hand-written" digits. In OmniInput, similar to the AUPR calculated from a dataset, a model with higher precision is anticipated to reduce susceptibility to overconfident predictions. Furthermore, a model with a higher AUPR is expected to align more closely with the desired input distribution of the training (testing) set.

Insights from Representative Inputs. An inspection of the representative inputs (Appendix G) reveals interesting insights. Firstly, different models exhibit distinct input-output mappings and preferences for specific types of inputs, indicating significant variations in their classification criteria. Specifically,

- MLP-MNIST-0/1 and MLP-AUG-MNIST-0/1 likely classify a background-foreground inverted digit "0" as "positive" (digit "1").
- CNN-MNIST-0/1 classifies inputs with a black background as positive.
- RES-GEN-MNIST-1, a generative model, demonstrates that it can map digits to large logit values.
- RES-AUG-MNIST-0/1, a classifier with data augmentation, demonstrates that adding noise during training help the model better map inputs that look like digit "1" to large logit values.

Moreover, RES-AUG-MNIST-0/1 exhibits relatively high recall as the representative inputs generally look like digit "1" with noise in the high logit regime. Conversely, RES-GEN-MNIST-1 generates more visually distinct inputs corresponding to the positive class, but with limited diversity in terms of noise variations.

These results suggest that generative training methods can improve the alignment between model predictions and human classification criteria, and underscore the need for enhancing recall in generative models. Adding noise to the data during training can also be beneficial.

Discussion. First, although OmniInput would regard CNN-MNIST-0/1 as a "bad" model, the digital "1" can still be found in the positive logit range. The low precision indicates the number of these informative digit inputs is so small that the model makes more overconfident predictions where the models map the obviously wrong instances (e.g. noisy images) over-confidently as "hand-written" digits. Having a mixture of poor-quality and high-quality inputs mapped to the same output indicates a flawed model, so further scrutiny of the inputs is required due to the uninformative and unreliable nature of the model's predictions. Second, the model does not use reliable features, such as "shapes" of the digits patterns to distinguish inputs. Had this model use shapes to achieve high accuracy, the representative inputs would have more similar patterns instead of unstructured or black backgrounds.

Third, the representative inputs of MLP-MNIST-0/1 and MLP-AUG-MNIST-0/1 display visual similarities, but the noise level decreases when the logit increases, indicating how noise affects the model's prediction. OmniInput finds this *distribution shift* in the representative inputs with regard to model outputs. Importantly, this distribution shift is presented by the model itself through the sampling step in OmniInput, without the need for manual trials and errors to find out the noise distribution (Hendrycks & Dietterich, 2019).

Together with the previous PR curve analysis, these findings suggest that different input-output mappings, along with the input distribution, are encoded in the models. This in turn affects the model performance. OmniInput is a novel way to gain insights into this, which can inform future research endeavors to focus on enhancing both robustness and visual diversity of the generative models.

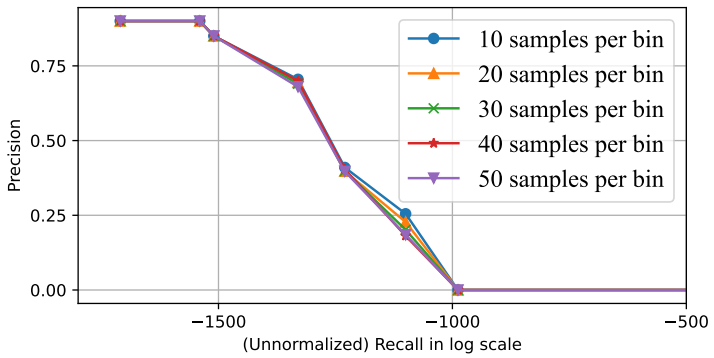

Figure 5: Convergence of OmniInput with respect to the number of annotated samples per bin. We use MLP-MNIST-0/1 as an example. There are 40 bins in total; each bin has at least 50 samples after deleting the duplicates.

Evaluation Effort, Efficiency, and Human Annotation Ambiguity. We have at least 50 samples per bin for all the models after deleting the duplicates. For a fixed sampling cost, the total num-

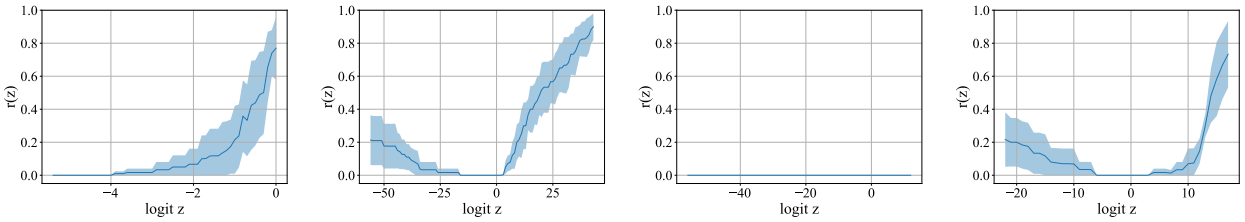

(a) RES-GEN-MNIST-1 (b) RES-AUG-MNIST-0/1 (c) CNN-MNIST-0/1 (d) MLP-MNIST-0/1

Figure 6: Precision per bin $r(z)$ with confidence intervals for four different models.

ber of samples is fixed. Hence a larger number of bins would result in fewer samples per bin. Evaluating these samples in our OmniInput framework requires less effort than annotating a dataset collected for traditional dataset-driven evaluation, e.g., 60000 annotations are needed for the MNIST.

In Fig. 5, we vary the number of annotated samples per bin in OmniInput from 10 to 50 and plot different precision-recall curves for the MLP-MNNIST-0/1 model. The results indicate that the evaluation converges quickly when the number of inputs approaches 40 or 50, empirically demonstrating that OmniInput requires relatively few annotated samples to reach a reliable evaluation.

We observe that models exhibit varying degrees of robustness and visual diversity. To assess the ambiguity in human labeling, we examine the variations in $r(z)$ when three different individuals label the same dataset (Fig. 6). Notably, apart from the CNN model, the other models display different levels of labeling ambiguity, i.e., different individuals label the same sample differently. These differences give the confidence intervals in the precision per bin, $r(z)$, and can be understood as the uncertainty of the model predictions.

4.4 Discussion on Model Annotation and Proposal Model Evaluation

Human Annotation vs. Model Annotation. In principle, metrics employed in evaluating generative models (Salimans et al., 2016; Heusel et al., 2017; Naeem et al., 2020; Sajjadi et al., 2018; Cheema & Urner, 2023) could be employed to obtain the $r(z)$ values in our method. However, relying on a performance-uncertified model in the entire input space to get $r(z)$ is inherently unreliable. We examined the Fréchet Inception Distance (FID) (Heusel et al., 2017), one of the most commonly used generative model performance metrics.

Feature extractors generate features from both the ground truth test set images and the images produced by the generative model, and then compares the distributional differences between these features. In our experiment, the ground truth inputs are test set digits from label=1.

The consistency of FID scores with human evaluations varies depending on the models and datasets. For example, in the case of RES-AUG-MNIST-0/1 (Table 2), a decrease in the FID score (indicating better performance) corresponds to an increase in the human score (also indicating better performance) as the logit value rises. This result suggests that certain metrics, like FID, may serve as substitutes for human annotations when evaluating generative models. However, for CNN-MNIST-0/1, the FID score can be entirely misleading. While human evaluators perceive the representative inputs of CNN-MNIST-0/1 for the logits in the table as unmeaningful (having a score of 0), the FID scores are similar to those of RES-AUG-MNIST-0/1, which contains meaningful digits. This is not the only inconsistent case between humans and metrics. For instance, the FID trend for MLP-MNIST-0/1 directly contradicts human intuition, as illustrated in Table 5 in Appendix F.

Table 2: Comparing human evaluations and FID scores as metrics of model performance. Although FID scores are similar for the two models, human labels differ significantly from the FID scores. OmniInput evaluates on the input space and thus the the evaluation is more consistent.

RES-AUG-MNIST-0/1			CNN-MNIST-0/1		
logits	humans↑	FID↓	logits	humans↑	FID↓
43	0.9	360.23	12	0	346.42
42	0.88	362.82	11	0	358.37
41	0.85	368.75	10	0	363.23
40	0.83	375.58	9	0	365.01

5 Related Works

Performance Characterization has been extensively studied in the literature (Haralick, 1992; Klette et al., 2000; Thacker et al., 2008; Ramesh et al., 1997; Bowyer & Phillips, 1998; Aghdasi, 1994; Ramesh & Haralick, 1992; 1994). Previous research focused on devising evaluation methods for specific model architectures, such as simple models (Hammitt & Bartlett, 1995) and mathematical morphological operators (Gao et al., 2002; Kanungo & Haralick, 1990). In our method, models can be a black box where the analytic characterization of the input-to-output function is unknown (Courtney et al., 1997; Cho et al., 1997), and we place emphasis on the output distribution (Greiffenhagen et al., 2001) to derive performance metrics. This approach allows us to evaluate the model's performance without requiring detailed knowledge of its internal workings. There are recent attempts (Qiu et al., 2020; Lang et al., 2021; Luo et al., 2023; Prabhu et al., 2023) to evaluate model performance without a pre-defined test set. These works used other generators to generate samples for evaluating the model. On the contrary, we use a sampler to sample from the model to be evaluated. Sampling is transparent with convergence estimates, but other generators are still used as black boxes. Because of the inherently unknown biases in generative models, utilizing these models to evaluate another model carries the risk of yielding unfair and potentially incorrect conclusions. Our method brings the focus back to the model to be tested, tasking it with generating samples by itself for scrutiny, rather than relying on external agents such as human or other models to come up with testing data. An additional benefit is that this approach offers a novel framework for estimating errors in the predictions when comparing different models.

Samplers MCMC samplers have gained widespread popularity in the machine learning community (Chen et al., 2014; Welling & Teh, 2011; Li et al., 2016; Xu et al., 2018). Among these, CSGLD (Deng et al., 2020) leverages the Wang–Landau algorithm (Wang & Landau, 2001) to comprehensively explore the energy landscape. Gibbs-With-Gradients (GWG)(Grathwohl et al., 2021) extends this approach to discrete domains, while discrete Langevin proposal (DLP)(Zhang et al., 2022) is able to propose global updates. Although these algorithms can in principle be used to sample the output distribution, they either require a long time to converge, or are not able to explore the full range of possible output values in our experience. We therefore employ parallel tempering (PT) with histogram reweighting (HR) to recover the full output distribution of the model, while ensuring a manageable time to solution.

Open-world Model Evaluation requires model to perform well for in-distribution test sets (Dosovitskiy et al., 2021; Tolstikhin et al., 2021; Steiner et al., 2021; Chen et al., 2021; Zhuang et al., 2022; He et al., 2015; Simonyan & Zisserman, 2014; Szegedy et al., 2015; Huang et al., 2017; Zagoruyko & Komodakis, 2016), OOD detection (Liu et al., 2020; Hendrycks & Gimpel, 2016; Hendrycks et al., 2019; Hsu et al., 2020; Lee et al., 2017; 2018; Liang et al., 2018; Mohseni et al., 2020; Ren et al., 2019), generalization (Cao et al., 2022; Sun & Li, 2022), and adversarial attacks (Szegedy et al., 2013; Rozsa et al., 2016; Miyato et al., 2018; Kurakin et al., 2016; Xie et al., 2019; Madry et al., 2017). Understanding performance of the model requires the consideration of an input space that includes all these types of samples.

6 Conclusions and Future Work

We present OmniInput, a novel framework for realizing dataset-free, comprehensive evaluations of models using Internet-scale data from the models' own input spaces. It is based on a new way to calculate the precision and recall by leveraging the output distribution. We demonstrate that OmniInput is applicable to a wide range of tasks, ranging from computer vision to natural language processing. Our work demonstrates the importance of sampling from the output distribution by showing how it enables the understanding of model's input-output mapping.

One important future work is to develop more efficient samplers for output distribution, so we can apply OmniInput for evaluating more complex models. It is also interesting to explore how to reduce the required amount of human annotation effort in model evaluations, especially when comparing two correlated models. We believe OmniInput opens the gate to many dataset-free evaluations in a near future and this is a crucial research direction especially in this LLM era when the benchmark dataset performance is less reliable for model comparison.

References

Farzin Aghdasi. *Digitization and analysis of mammographic images for early detection of breast cancer*. PhD thesis, University of British Columbia, 1994.

Kevin Bowyer and P Jonathon Phillips. *Empirical evaluation techniques in computer vision*. IEEE Computer Society Press, 1998.

Kaidi Cao, Maria Brbic, and Jure Leskovec. Open-world semi-supervised learning. In *International Conference on Learning Representations*, 2022. URL `https://openreview.net/forum?id=O-r8LOR-CCA`.

Fasil Cheema and Ruth Urner. Precision recall cover: A method for assessing generative models. In Francisco Ruiz, Jennifer Dy, and Jan-Willem van de Meent (eds.), *Proceedings of The 26th International Conference on Artificial Intelligence and Statistics*, volume 206 of *Proceedings of Machine Learning Research*, pp. 6571–6594. PMLR, 25–27 Apr 2023. URL `https://proceedings.mlr.press/v206/cheema23a.html`.

Tianqi Chen, Emily Fox, and Carlos Guestrin. Stochastic gradient hamiltonian monte carlo. In *International conference on machine learning*, pp. 1683–1691. PMLR, 2014.

Xiangning Chen, Cho-Jui Hsieh, and Boqing Gong. When vision transformers outperform resnets without pretraining or strong data augmentations. *arXiv preprint arXiv:2106.01548*, 2021.

Kyujin Cho, Peter Meer, and Javier Cabrera. Performance assessment through bootstrap. *IEEE Transactions on Pattern Analysis and Machine Intelligence*, 19(11):1185–1198, 1997.

Tarin Clanuwat, Mikel Bober-Irizar, Asanobu Kitamoto, Alex Lamb, Kazuaki Yamamoto, and David Ha. Deep learning for classical japanese literature, 2018.

Gregory Cohen, Saeed Afshar, Jonathan Tapson, and Andre Van Schaik. Emnist: Extending mnist to handwritten letters. *2017 International Joint Conference on Neural Networks (IJCNN)*, 2017. doi: 10.1109/ijcnn.2017.7966217.

Patrick Courtney, Neil Thacker, and Adrian F Clark. Algorithmic modelling for performance evaluation. *Machine Vision and Applications*, 9(5):219–228, 1997.

Wei Deng, Guang Lin, and Faming Liang. A contour stochastic gradient langevin dynamics algorithm for simulations of multi-modal distributions. In *Advances in Neural Information Processing Systems*, 2020.

Alexey Dosovitskiy, Lucas Beyer, Alexander Kolesnikov, Dirk Weissenborn, Xiaohua Zhai, Thomas Unterthiner, Mostafa Dehghani, Matthias Minderer, Georg Heigold, Sylvain Gelly, Jakob Uszkoreit, and Neil Houlsby. An image is worth 16x16 words: Transformers for image recognition at scale. *ICLR*, 2021.

Alan M. Ferrenberg and Robert H. Swendsen. Optimized Monte Carlo data analysis. *Physical Review Letters*, 63(12):1195–1198, September 1989. doi: 10.1103/PhysRevLett.63.1195.

Xiang Gao, Visvanathan Ramesh, and Terry Boult. Statistical characterization of morphological operator sequences. In *European Conference on Computer Vision*, pp. 590–605. Springer, 2002.

Katayoon Goshvadi, Haoran Sun, Xingchao Liu, Azade Nova, Ruqi Zhang, Will Grathwohl, Dale Schuurmans, and Hanjun Dai. Discs: a benchmark for discrete sampling. *Advances in Neural Information Processing Systems*, 36, 2024.

Will Grathwohl, Kevin Swersky, Milad Hashemi, David Duvenaud, and Chris Maddison. Oops i took a gradient: Scalable sampling for discrete distributions. In *International Conference on Machine Learning*, pp. 3831–3841. PMLR, 2021.

Michael Greiffenhagen, Dorin Comaniciu, Heinrich Niemann, and Visvanathan Ramesh. Design, analysis, and engineering of video monitoring systems: An approach and a case study. *Proceedings of the IEEE*, 89 (10):1498–1517, 2001.

Dirk Groeneveld, Iz Beltagy, Pete Walsh, Akshita Bhagia, Rodney Kinney, Oyvind Tafjord, A. Jha, Hamish Ivison, Ian Magnusson, Yizhong Wang, Shane Arora, David Atkinson, Russell Authur, Khyathi Raghavi Chandu, Arman Cohan, Jennifer Dumas, Yanai Elazar, Yuling Gu, Jack Hessel, Tushar Khot, William Merrill, Jacob Daniel Morrison, Niklas Muennighoff, Aakanksha Naik, Crystal Nam, Matthew E. Peters, Valentina Pyatkin, Abhilasha Ravichander, Dustin Schwenk, Saurabh Shah, Will Smith, Emma Strubell, Nishant Subramani, Mitchell Wortsman, Pradeep Dasigi, Nathan Lambert, Kyle Richardson, Luke Zettlemoyer, Jesse Dodge, Kyle Lo, Luca Soldaini, Noah A. Smith, and Hanna Hajishirzi. Olmo: Accelerating the science of language models. *arXiv preprint*, 2024. URL `https://api.semanticscholar.org/CorpusID:267365485`.

AM Hammitt and EB Bartlett. Determining functional relationships from trained neural networks. *Mathematical and computer modelling*, 22(3):83–103, 1995.

Robert M Haralick. Performance characterization in computer vision. In *BMVC92*, pp. 1–8. Springer, 1992.

Kaiming He, Xiangyu Zhang, Shaoqing Ren, and Jian Sun. Deep residual learning for image recognition. *arXiv preprint arXiv:1512.03385*, 2015.

Dan Hendrycks and Thomas Dietterich. Benchmarking neural network robustness to common corruptions and perturbations. *Proceedings of the International Conference on Learning Representations*, 2019.

Dan Hendrycks and Kevin Gimpel. A baseline for detecting misclassified and out-of-distribution examples in neural networks. *arXiv preprint arXiv:1610.02136*, 2016.

Dan Hendrycks, Mantas Mazeika, and Thomas Dietterich. Deep anomaly detection with outlier exposure. In *International Conference on Learning Representations*, 2019. URL `https://openreview.net/forum?id=HyxCxhRcY7`.

Martin Heusel, Hubert Ramsauer, Thomas Unterthiner, Bernhard Nessler, and Sepp Hochreiter. Gans trained by a two time-scale update rule converge to a local nash equilibrium. *Advances in neural information processing systems*, 30, 2017.

Ari Holtzman, Jan Buys, Li Du, Maxwell Forbes, and Yejin Choi. The curious case of neural text degeneration. *arXiv preprint arXiv:1904.09751*, 2019.

Yen-Chang Hsu, Yilin Shen, Hongxia Jin, and Zsolt Kira. Generalized ODIN: Detecting out-of-distribution image without learning from out-of-distribution data. In *Proceedings of the IEEE/CVF Conference on Computer Vision and Pattern Recognition*, pp. 10951–10960, 2020.

Gao Huang, Zhuang Liu, Laurens Van Der Maaten, and Kilian Q Weinberger. Densely connected convolutional networks. In *Proceedings of the IEEE conference on computer vision and pattern recognition*, pp. 4700–4708, 2017.

Koji Hukushima and Koji Nemoto. Exchange monte carlo method and application to spin glass simulations. *Journal of the Physical Society of Japan*, 65(6):1604–1608, 1996.

Tapas Kanungo and Robert M Haralick. Character recognition using mathematical morphology. In *Proc. of the Fourth USPS Conference on Advanced Technology*, pp. 973–986, 1990.

Reinhard Klette, H Siegfried Stiehl, Max A Viergever, and Koen L Vincken. *Performance characterization in computer vision*. Springer, 2000.

Sachin Kumar, Biswajit Paria, and Yulia Tsvetkov. Constrained sampling from language models via langevin dynamics in embedding spaces. In *Proceedings of the 2022 Conference on Empirical Methods in Natural Language Processing (EMNLP)*, 2022.

Alexey Kurakin, Ian Goodfellow, Samy Bengio, et al. Adversarial examples in the physical world, 2016.

DP Landau, Shan-Ho Tsai, and M Exler. A new approach to monte carlo simulations in statistical physics: Wang-landau sampling. *American Journal of Physics*, 72(10):1294–1302, 2004.

Oran Lang, Yossi Gandelsman, Michal Yarom, Yoav Wald, Gal Elidan, Avinatan Hassidim, William T. Freeman, Phillip Isola, Amir Globerson, Michal Irani, and Inbar Mosseri. Explaining in style: Training a gan to explain a classifier in stylespace. *arXiv preprint arXiv:2104.13369*, 2021.

Guillaume Leclerc, Hadi Salman, Andrew Ilyas, Sai Vemprala, Logan Engstrom, Vibhav Vineet, Kai Xiao, Pengchuan Zhang, Shibani Santurkar, Greg Yang, et al. 3db: A framework for debugging computer vision models. *Advances in Neural Information Processing Systems*, 35:8498–8511, 2022.

Yann LeCun, Sumit Chopra, Raia Hadsell, M Ranzato, and Fujie Huang. A tutorial on energy-based learning. *Predicting structured data*, 1(0), 2006.

Kimin Lee, Honglak Lee, Kibok Lee, and Jinwoo Shin. Training confidence-calibrated classifiers for detecting out-of-distribution samples. *arXiv preprint arXiv:1711.09325*, 2017.

Kimin Lee, Kibok Lee, Honglak Lee, and Jinwoo Shin. A simple unified framework for detecting out-of-distribution samples and adversarial attacks. In *Advances in Neural Information Processing Systems*, pp. 7167–7177, 2018.

Chunyuan Li, Changyou Chen, David Carlson, and Lawrence Carin. Preconditioned stochastic gradient langevin dynamics for deep neural networks. In *Thirtieth AAAI Conference on Artificial Intelligence*, 2016.

Shiyu Liang, Yixuan Li, and Rayadurgam Srikant. Enhancing the reliability of out-of-distribution image detection in neural networks. In *6th International Conference on Learning Representations, ICLR 2018*, 2018.

Weitang Liu, Xiaoyun Wang, John Owens, and Yixuan Li. Energy-based out-of-distribution detection. *Advances in Neural Information Processing Systems*, 2020.

Weitang Liu, Yi-Zhuang You, Ying Wai Li, and Jingbo Shang. Gradient-based wang-landau algorithm: A novel sampler for output distribution of neural networks over the input space. In Andreas Krause, Emma Brunskill, Kyunghyun Cho, Barbara Engelhardt, Sivan Sabato, and Jonathan Scarlett (eds.), *Proceedings of the 40th International Conference on Machine Learning*, volume 202 of *Proceedings of Machine Learning Research*, pp. 22338–22351. PMLR, 23–29 Jul 2023. URL `https://proceedings.mlr.press/v202/liu23aw.html`.

Jinqi Luo, Zhaoning Wang, Chen Henry Wu, Dong Huang, and Fernando De La Torre. Zero-shot model diagnosis. In *Proceedings of the IEEE/CVF Conference on Computer Vision and Pattern Recognition (CVPR)*, 2023.

Aleksander Madry, Aleksandar Makelov, Ludwig Schmidt, Dimitris Tsipras, and Adrian Vladu. Towards deep learning models resistant to adversarial attacks. *arXiv preprint arXiv:1706.06083*, 2017.

Nicholas Metropolis, Arianna W. Rosenbluth, Marshall N. Rosenbluth, Augusta H. Teller, and Edward Teller. Equation of State Calculations by Fast Computing Machines. *The Journal of Chemical Physics*, 21(6):1087–1092, June 1953. ISSN 0021-9606. doi: 10.1063/1.1699114.

Takeru Miyato, Shin-ichi Maeda, Masanori Koyama, and Shin Ishii. Virtual adversarial training: a regularization method for supervised and semi-supervised learning. *IEEE transactions on pattern analysis and machine intelligence*, 41(8):1979–1993, 2018.

Sina Mohseni, Mandar Pitale, JBS Yadawa, and Zhangyang Wang. Self-supervised learning for generalizable out-of-distribution detection. *Proceedings of the AAAI Conference on Artificial Intelligence*, 34(04): 5216–5223, April 2020. ISSN 2159-5399. doi: 10.1609/aaai.v34i04.5966.

Muhammad Ferjad Naeem, Seong Joon Oh, Youngjung Uh, Yunjey Choi, and Jaejun Yoo. Reliable fidelity and diversity metrics for generative models. 2020.

Viraj Prabhu, Sriram Yenamandra, Prithvijit Chattopadhyay, and Judy Hoffman. Lance: Stress-testing visual models by generating language-guided counterfactual images. In *Neural Information Processing Systems (NeurIPS)*, 2023.

Lianhui Qin, Sean Welleck, Daniel Khashabi, and Yejin Choi. Cold decoding: Energy-based constrained text generation with langevin dynamics. *Advances in Neural Information Processing Systems*, 35:9538–9551, 2022.

Haonan Qiu, Chaowei Xiao, Lei Yang, Xinchen Yan, Honglak Lee, and Bo Li. Semanticadv: Generating adversarial examples via attribute-conditioned image editing. In *ECCV*, 2020.

Alec Radford, Jeff Wu, Rewon Child, David Luan, Dario Amodei, and Ilya Sutskever. Language models are unsupervised multitask learners. 2019.

V Ramesh and RM Haralick. A methodology for automatic selection of iu algorithm tuning parameters. In *ARPA Image Understanding Workshop*, 1994.

Visvanathan Ramesh and Robert M Haralick. Random perturbation models and performance characterization in computer vision. In *Proceedings 1992 IEEE Computer Society Conference on Computer Vision and Pattern Recognition*, pp. 521–522. IEEE Computer Society, 1992.

Visvanathan Ramesh, RM Haralick, AS Bedekar, X Liu, DC Nadadur, KB Thornton, and X Zhang. Computer vision performance characterization. *RADIUS: Image Understanding for Imagery Intelligence*, pp. 241–282, 1997.

Jie Ren, Peter J Liu, Emily Fertig, Jasper Snoek, Ryan Poplin, Mark Depristo, Joshua Dillon, and Balaji Lakshminarayanan. Likelihood ratios for out-of-distribution detection. In *Advances in Neural Information Processing Systems*, pp. 14680–14691, 2019.

Andras Rozsa, Ethan M Rudd, and Terrance E Boult. Adversarial diversity and hard positive generation. In *Proceedings of the IEEE Conference on Computer Vision and Pattern Recognition Workshops*, pp. 25–32, 2016.

Mehdi S. M. Sajjadi, Olivier Bachem, Mario Lučić, Olivier Bousquet, and Sylvain Gelly. Assessing Generative Models via Precision and Recall. In *Advances in Neural Information Processing Systems (NeurIPS)*, 2018.

Tim Salimans, Ian Goodfellow, Wojciech Zaremba, Vicki Cheung, Alec Radford, and Xi Chen. Improved techniques for training gans. *Advances in neural information processing systems*, 29, 2016.

V Sanh. Distilbert, a distilled version of bert: smaller, faster, cheaper and lighter. *arXiv preprint arXiv:1910.01108*, 2019.

Victor Sanh, Lysandre Debut, Julien Chaumond, and Thomas Wolf. Distilbert, a distilled version of bert: smaller, faster, cheaper and lighter. *ArXiv*, abs/1910.01108, 2019.

Michelle Shu, Chenxi Liu, Weichao Qiu, and Alan Yuille. Identifying model weakness with adversarial examiner. In *Proceedings of the AAAI conference on artificial intelligence*, volume 34, pp. 11998–12006, 2020.

Karen Simonyan and Andrew Zisserman. Very deep convolutional networks for large-scale image recognition. *arXiv preprint arXiv:1409.1556*, 2014.

Richard Socher, Alex Perelygin, Jean Wu, Jason Chuang, Christopher D. Manning, Andrew Ng, and Christopher Potts. Recursive deep models for semantic compositionality over a sentiment treebank. In *Proceedings of the 2013 Conference on Empirical Methods in Natural Language Processing*, pp. 1631–1642, Seattle, Washington, USA, October 2013. Association for Computational Linguistics. URL `https://www.aclweb.org/anthology/D13-1170`.

Andreas Steiner, Alexander Kolesnikov, , Xiaohua Zhai, Ross Wightman, Jakob Uszkoreit, and Lucas Beyer. How to train your vit? data, augmentation, and regularization in vision transformers. *arXiv preprint arXiv:2106.10270*, 2021.

Yiyou Sun and Yixuan Li. Open-world contrastive learning. *arXiv preprint arXiv:2208.02764*, 2022.

Robert H Swendsen and Jian-Sheng Wang. Replica monte carlo simulation of spin-glasses. *Physical review letters*, 57(21):2607, 1986.

Christian Szegedy, Wojciech Zaremba, Ilya Sutskever, Joan Bruna, Dumitru Erhan, Ian Goodfellow, and Rob Fergus. Intriguing properties of neural networks. *arXiv preprint arXiv:1312.6199*, 2013.

Christian Szegedy, Wei Liu, Yangqing Jia, Pierre Sermanet, Scott Reed, Dragomir Anguelov, Dumitru Erhan, Vincent Vanhoucke, and Andrew Rabinovich. Going deeper with convolutions. In *Proceedings of the IEEE conference on computer vision and pattern recognition*, pp. 1–9, 2015.

Neil A Thacker, Adrian F Clark, John L Barron, J Ross Beveridge, Patrick Courtney, William R Crum, Visvanathan Ramesh, and Christine Clark. Performance characterization in computer vision: A guide to best practices. *Computer vision and image understanding*, 109(3):305–334, 2008.

Ilya Tolstikhin, Neil Houlsby, Alexander Kolesnikov, Lucas Beyer, Xiaohua Zhai, Thomas Unterthiner, Jessica Yung, Andreas Steiner, Daniel Keysers, Jakob Uszkoreit, Mario Lucic, and Alexey Dosovitskiy. Mlp-mixer: An all-mlp architecture for vision. *arXiv preprint arXiv:2105.01601*, 2021.

Fugao Wang and David P Landau. Efficient, multiple-range random walk algorithm to calculate the density of states. *Physical review letters*, 86(10):2050, 2001.

Max Welling and Yee W Teh. Bayesian learning via stochastic gradient langevin dynamics. In *Proceedings of the 28th international conference on machine learning (ICML-11)*, pp. 681–688, 2011.

Han Xiao, Kashif Rasul, and Roland Vollgraf. Fashion-mnist: a novel image dataset for benchmarking machine learning algorithms, 2017.

Cihang Xie, Zhishuai Zhang, Yuyin Zhou, Song Bai, Jianyu Wang, Zhou Ren, and Alan L Yuille. Improving transferability of adversarial examples with input diversity. In *Proceedings of the IEEE/CVF Conference on Computer Vision and Pattern Recognition*, pp. 2730–2739, 2019.

Pan Xu, Jinghui Chen, Difan Zou, and Quanquan Gu. Global convergence of langevin dynamics based algorithms for nonconvex optimization. *Advances in Neural Information Processing Systems*, 31, 2018.

Chhavi Yadav and Léon Bottou. Cold case: The lost mnist digits. In *Advances in Neural Information Processing Systems 32*. Curran Associates, Inc., 2019.

Sergey Zagoruyko and Nikos Komodakis. Wide residual networks. *arXiv preprint arXiv:1605.07146*, 2016.

Ruqi Zhang, Xingchao Liu, and Qiang Liu. A langevin-like sampler for discrete distributions. *International Conference on Machine Learning*, 2022.

Juntang Zhuang, Boqing Gong, Liangzhe Yuan, Yin Cui, Hartwig Adam, Nicha Dvornek, Sekhar Tatikonda, James Duncan, and Ting Liu. Surrogate gap minimization improves sharpness-aware training. *ICLR*, 2022.

A Connection between ROC and PR curve in the input space

It is common in the traditional evaluation framework to consider the receiver operating characteristic curve (ROC) and precision-recall (PR) separately. The recall in PR is the same as the unnormalized true positive

rate in ROC, so we do not need to consider the true positive rate separately. The false positive is the number of positively predicted inputs minus the number of the true positives (using the notation of Equ. 3)

$$\sum_{z\geq\lambda}^{+\infty}\rho(z)-\sum_{z\geq\lambda}^{+\infty}r(z)\rho(z)=\sum_{z\geq\lambda}^{+\infty}\rho(z)(1-r(z))$$

The false positive rate is the number of false positives divided by the number of inputs of the negative class. Since the number of inputs of the negative class is a constant in the input space, the unnormalized false positive rate is:

$$\text{False positive rate}\propto\sum_{z\geq\lambda}^{+\infty}\rho(z)(1-r(z)).$$

In other words, once we compute the true positive, the false positive rate is simply proportional to the false positive ($\sum_{z\geq\lambda}^{+\infty}\rho(z)-$ true positive) in the input space. Thus, plotting the ROC curve is like plotting $1-r(z)$ and $r(z)$ scaled by $\rho(z)$ respectively. Comparing the equation of the (unnormalized) recall, this (unnormalized) false positive rate contains (almost if not all) the same information as the (unnormalized) recall in the input space.

B PR curves for OLMOo models

Fig. 7 shows the PR curves for OLMo-7B, OLMo-7B-Instrct, OLMo-7B-SFT and OLMo-1B.

C Language Classifier

For sentence length 66, some sampled inputs with logit equals 7 (positive sentiment) in Fig 8.

For sentence length 10, some sampled inputs with logit equals 7 (positive sentiment) in Fig 9.

D Details of the Computer Vision Models used in Evaluation

The ResNet used in our experiments is the same as the one used in GWG (Grathwohl et al., 2021). For the input pixels, we employ one-hot encoding and transform them into a 3-channel output through a 3-by-3 convolutional layer. The resulting output is then processed by the backbone models to generate features. The CNN backbone consists of two 2-layer 3-by-3 convolutional filters with 32 and 128 output channels, respectively. The MLP backbone comprises a single hidden layer with flattened images as inputs and produced 128-dimensional features as output. All the features from the backbone models are ultimately passed through a fully-connected layer to generate a scalar output.

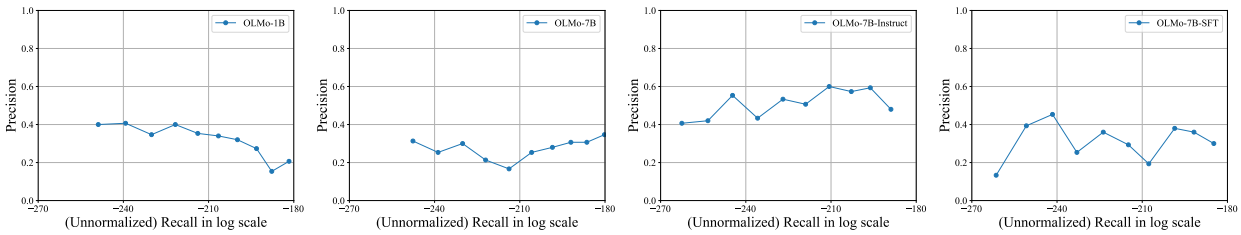

(a) PR for OLMo-1B. (b) PR for OLMo-7B. (c) PR for OLMo-7B-Instruct. (d) PR for OLMo-7B-SFT.

Figure 7: PR for OLMo Language models.

['[CLS]', 'positive', 'dazzling', 'textual', 'quilt', 'shale', 'funk', 'austro', 'advanced', 'tending', 'animals', 'grasping', 'mann', 'scott', 'lower', 'knives', 'avant', 'luckily', '##gui', 'nations', '##48', 'lions', 'nixon', 'steer', 'instituted', 'mont', '##uo', 'hang', 'muir', 'dublin', 'armchair', 'lips', '##tin', 'pianist', 'introduce', '.', 'gunn', 'rosenberg', 'sarawak', 'eddy', '##manship', 'deluxe', 'highway', '##gaard', 'entertain', 'chronic', '##jing', 'objects', 'sw', '##flies', '##tri', 'root', '##phone', 'franciscan', 'longitudinal', 'dealing', 'emilio', 'godfrey', 'audiences', 'comparison', 'shards', 'friendship', 'emphasized', '##ssel', '##ssen', '[SEP]']

['[CLS]', 'positive', 'dazzling', 'textual', 'quilt', 'skill', 'animal', 'fein', 'jocelyn', 'compelling', 'bounce', '##rson', 'mcgraw', 'dynasty', 'buy', '##fight', '##ʊ', 'republics', 'fictional', '##umble', 'spaniards', 'ronnie', 'wise', 'baha', 'chefs', 'flipping', 'pa', 'symphonies', '##ryn', 'seaman', '##bler', '##ia', '##3', '##tius', 'nests', '.', 'growing', 'phosphorus', 'stakes', '##wski', 'penalty', 'killers', 'manages', '##hue', '##tions', '##rval', 'modify', '##rong', 'bikes', 'frankenstein', 'hayden', 'shirt', 'satisfaction', 'taylor', 'modes', 'audiences', 'impact', '##ska', 'shirley', 'albanians', 'playboy', 'extensions', 'mongolian', 'saturn', '1692', '[SEP]']

['[CLS]', 'positive', 'dazzling', 'textual', 'coloring', 'lays', 'bsc', 'fold', 'michael', 'metre', '332', 'herself', 'von', 'silhouette', 'protestant', 'sonata', 'emblem', 'rag', 'fictional', 'lb', 'yours', 'generator', 'chorale', 'kits', 'marine', '##haya', '##rdes', 'aegean', '350', 'jailed', 'sucks', 'magical', 'graveyard', 'fragile', '##oco', 'hostage', 'honestly', 'retirement', 'wiley', 'interpreted', '‘', '##ooping', '##sat', 'devices', 'domesday', 'animation', 'nokia', 'doctoral', 'erich', 'prefix', 'nectar', 'telling', 'wrapping', '##ight', 'herrera', 'fiona', 'stella', 'various', 'since', 'レ', 'arcade', 'passengers', 'terrace', 'newcastle', 'impact', '[SEP]']

['[CLS]', 'positive', 'dazzling', 'textual', 'coloring', 'izzy', 'fisher', 'housing', 'knock', 'supplier', 'park', 'cigar', 'costume', 'essay', 'maple', 'cemetery', 'walton', 'herman', 'like', 'ethernet', 'strikeouts', '花', 'reconstruction', 'distal', '##rien', 'asking', 'choral', 'adventures', '»', 'nucleus', 'accounts', '102', 'illinois', 'is', 'luna', 'hostage', 'clans', 'shit', 'seventeen', '##²', 'canterbury', 'semiconductor', 'childbirth', 'cock', '##iza', 'themed', 'elmer', 'jin', 'ヤ', '##uta', 'cordoba', 'palatine', 'moose', 'dir', 'passenger', 'teller', 'craters', '1710', 'yearbook', 'ɳ', 'jude', 'decades', '##cards', 'santana', '##ume', '[SEP]']

['[CLS]', 'genuinely', 'dazzling', 'textual', 'streaks', '##quist', 'founders', 'generals', 'khan', '##st', 'mahogany', '##evich', 'rwanda', 'penguin', 'bobbed', 'detroit', 'anwar', 'oppression', '##hak', '##isches', 'salmon', '##rien', 'deportation', 'flirt', 'mongolian', '##brush', 'second', 'adventures', 'liquids', 'birth', 'traditional', 'turned', 'induced', 'philharmonic', 'swept', 'stallion', 'geometridae', 'mohan', 'thoughts', '##onga', 'bullock', 'mourning', 'wei', 'teen', 'knighted', 'bavaria', 'atkins', 'peterson', 'ud', 'corona', 'gripped', 'strands', '##iel', 'barclay', 'arranged', 'pune', 'wraps', 'at', 'clues', 'ether', 'strait', 'czechoslovakia', '##rith', 'son', '##glia', '[SEP]']

Figure 8: Sampled inputs of SST2 with sentence length 66.

['[CLS]', 'brave', 'searing', 'vivid', 'nbl', 'restoring', 'uploaded', 'sleeps', 'loyalists', '[SEP]']
['[CLS]', 'appreciated', 'shattering', 'nile', 'barack', 'branch', 'lifelong', 'flavor', 'cow', '[SEP]']
['[CLS]', 'incredibly', 'refreshing', '勝', 'transport', 'teddy', 'fledgling', 'μ', '##pie', '[SEP]']
['[CLS]', 'lexington', 'band', 'difficult', 'prophets', 'humanitarian', 'bianca', 'detectives', 'beautifully', '[SEP]']
['[CLS]', 'made', '##onzo', 'folklore', 'extraordinary', 'islands', 'gameplay', 'absolutely', 'summons', '[SEP]']
['[CLS]', 'generous', 'acceleration', 'precision', '1792', 'freiburg', 'signature', 'treasure', 'parkinson', '[SEP]']
['[CLS]', 'vibrant', 'keen', 'aboriginal', 'psychiatrist', 'scott', 'monumental', '##tical', '1920', '[SEP]']
['[CLS]', 'contraction', 'businessman', 'sunderland', '##away', 'jewelry', 'harmony', 'inspiring', 'realistic', '[SEP]']

Figure 9: Sampled inputs of SST2 with sentence length 10.

E Traditional Model Evaluation Results

Tab. 3 shows the AUROC of different models based on pre-defined test sets with different negative class(es). The MLP-MNIST-0/1 performs better on Fashion MNIST but worse in the rest than RES-AUG-MNIST-0/1. RES-GEN-MNIST-1 usually perform the best. CNN-MNIST-0/1 performs better in Kuzushiji MNIST

than RES-AUG-MNIST-0/1 and MLP-MNIST-0/1 but worse on the rest. Tab 4 shows the FPR95 results. CNN-MNIST-0/1 performs better on Kuzushiji MNIST than RES-AUG-MNIST-0/1 and MLP-MNIST-0/1 but worse on the rest. These results show the inconsistency between the metrics, dataset and the models.

Test Set	class=0 (in-dist)	Fashion MNIST (OOD)	Kuzushiji MNIST (OOD)	EMNIST (OOD)	QMNIST (OOD)
CNN-MNIST-0/1	99.76	99.88	99.31	99.56	92.46
RES-GEN-MNIST-1†	99.99	100.00	100.00	100.00	94.85
RES-AUG-MNIST-0/1	100.00	99.91	99.15	99.93	94.32
MLP-MNIST-0/1	100.00	99.93	98.62	99.83	94.17

†Class=0 is OOD for GEN model.

Table 3: AUROC. The higher the better.

Test Set	class=0 (in-dist)	Fashion MNIST (OOD)	Kuzushiji MNIST (OOD)	EMNIST (OOD)	QMNIST (OOD)
CNN-MNIST-0/1	0.54	0.51	2.78	1.98	21.08
RES-GEN-MNIST-1†	0.00	0.00	0.00	0.00	10.55
RES-AUG-MNIST-0/1	0.00	0.34	4.60	0.31	14.17
MLP-MNIST-0/1	0.00	0.27	6.68	0.64	13.24

†Class=0 is OOD for GEN model.

Table 4: FPR95. The lower the better.

F Human-metrics inconsistency

In table 5 of MLP-MNIST-0/1, the FID scores indicate the samples are bad when humans think they are good. The FID scores indicate the even better performance (lower scores) in the logit ranges when humans label as incorrect in general.

When the logits are large, humans label the representative inputs as "1." When the logits are small, representative inputs look like "0." However, the FID scores are better for these "0" inputs, indicating the feature extractors believe these "0" inputs look more like digits "1." The key contradiction is that the feature extractors of these metrics, when trained on certain datasets, are not verified to be applicable to all OOD settings, but surely they will be applied in OOD settings to generate features of inputs from models for evaluation. It is difficult to ensure they will perform reliably.

logits	humans↑	FID↓
17	0.73	434.32
16	0.67	436.60
15	0.58	432.89
14	0.48	430.79
-19	0.18	422.01
-20	0.2	419.94
-21	0.2	412.96
-22	0.216	405.20

Table 5: For MLP-MNIST-0/1, the FID scores indicate the samples are bad when humans think they are good. The FID scores indicate the even better performance (lower scores) in the logit ranges when humans label as incorrect in general.

G Representative inputs for MNIST images

Representative inputs for different models are in Fig. 10.

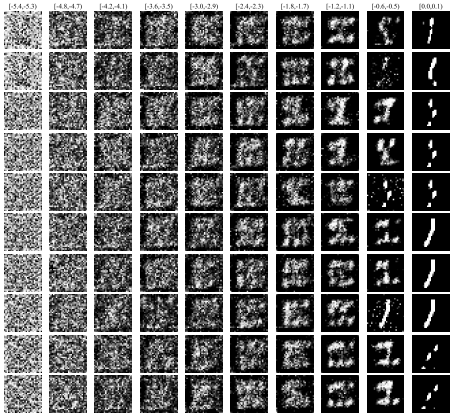

(a) RES-GEN-MNIST-1

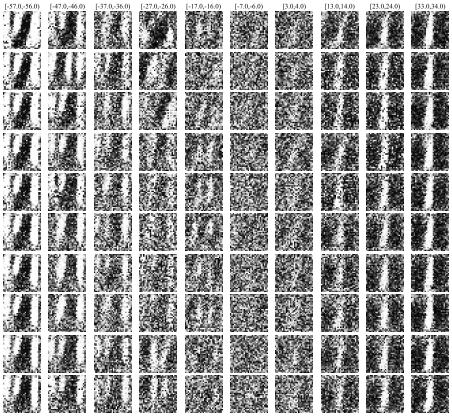

(b) RES-AUG-MNIST-0/1

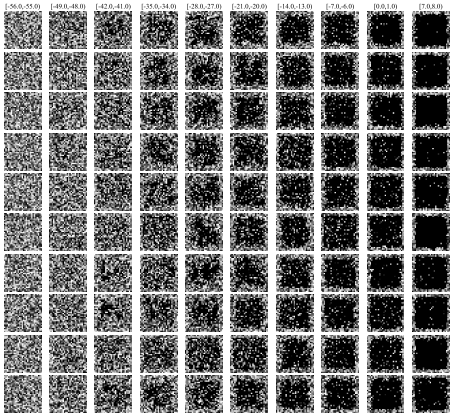

(c) CNN-MNIST-0/1

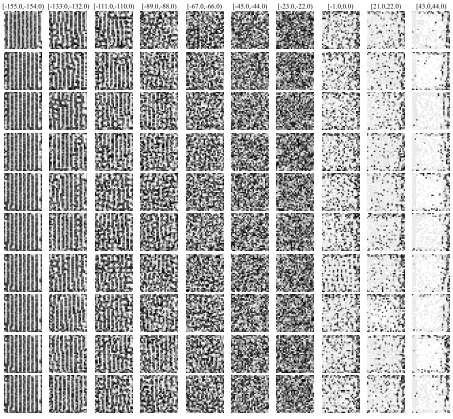

(d) CNN-AUG-MNIST-0/1

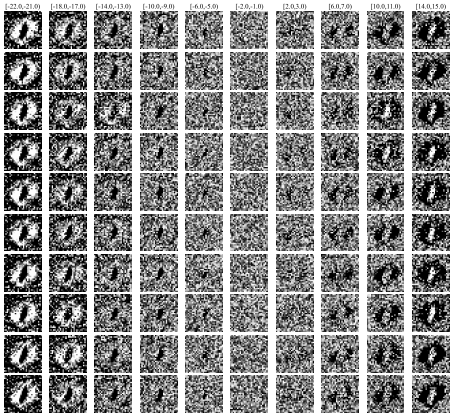

(e) MLP-MNIST-0/1

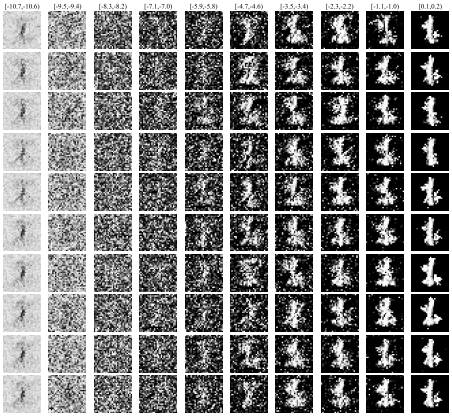

(f) MLP-GEN-MNIST-1

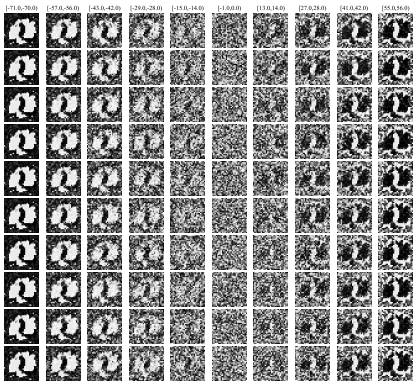

(g) MLP-AUG-MNIST-0/1

Figure 10: Representative inputs of different models.

H Example sampled inputs of (Large) Language models

We include a few example samples for GPT2 and OlMo in Tab. 6.

Model	NLL	Samples
GPT2-small-25	1.5	stores, grocery stores, restaurants, grocery stores, grocery stores, grocery stores, grocery shopping centers, supermarkets, restaurants, grocery
GPT2-small-25	2.0	science, science fiction and science-fiction films, Final Fantasy VII, and The Lord of the Rings, among other titles.
GPT2-small-25	2.5	Dean was really nice and kind. He was sort of a cuddly. I love him, he's such a good
GPT2-small-25	3.0	ethnic tendencies. Students continue to be taught that their current situation is their own fault and they should be taken to task for it
GPT2-small-25	3.2	The band responded that they do not refer to themselves as "old school," but rather as modern-era
GPT2-small-25	3.5	lure Daphne, Harry. Now our world knows Hermione Granger wasn't the only person in the school who was kidnapped.
GPT2-small-25	4.0	Flags and weight fluctuations in the water with power plants and dissipating energy put a lot of strain on the water control system because
GPT2-medium-25	1.7	houses, government buildings, schools, hospitals, and other buildings used for public purposes, such as airports, military bases, and
GPT2-medium-25	2.0	sadness, but it's a good feeling, and there's a sense that we're better because of it. And that's
GPT2-medium-25	2.5	Communists were trying to re-create the experiences of the American Civil War where black soldiers fought alongside white soldiers and played a crucial
GPT2-medium-25	3.0	drastically altered. In the early monastic period the belief in eternal life and free will had been transformed into a religious belief in
GPT2-medium-25	3.2	acknowledging the wickedness of man due to him, in venting his indignation against him and finally cursing him, he says
GPT2-medium-25	3.5	consequence that Chinese law enforcement is very unclear. In fact, given the lack of clear territorial boundaries and with respect to whom the
GPT2-medium-25	4.0	disqualifications from Supreme Court proceedings, defence from prosecution, compelment of guardians, obligation to pay retainer of one half
OLMo-1B	3.0	abouts demeasure on what is to be thereupon upon upon upon upon upon also also also also also also too too
OLMo-1B	3.5	analys anding several changes and adaptations in human brains and their evolution throughout the world history. Brain evolution study discusses how the brain
OLMo-1B	3.8	farmers traditional ways of life/culture is not acceptable. It comes out from talking which points out the issue of racism, sex
OLMo-1B	4.5	cis chooses to establish her identity with the Autotaschusansa society," in which typically feminine aspects are a fundamental part
OLMo-7B	3.0	vp@b v pvphv-p c-a v pvpbv-cpv c-vpv
OLMo-7B	3.5	wei's C2H probe demonstrated the excellent Ln sensitivity and the low detection limit of Ln. A variety of L
OLMo-7B	3.8	Whatever happens outcome his ego and character endures it his name will forever thereafter be live in history as it's it's the
OLMo-7B-Instruct	4.0	Devil and Parker Brothers, for poorly made games which often were inaccessible for children, partly due to the strict licensing rules. As
OLMo-7B-Instruct	4.5	requisite kms which is all about home address details, favourite foods and what sounds psychical. You will be found that you
OLMo-7B-SFT	3.5	memory models more often tend towards simple models that treat memory capacity as uniform across all types of memory content. RY: I
OLMo-7B-SFT	4.0	Something people including me can do.! Creative and idea generating workshops can help you when you need something new for a project

Table 6: Example Samples